Construction and Building Materials 415 (2024) 135055

Contents lists available at ScienceDirect

Construction and Building Materials

journal homepage: www.elsevier.com/locate/conbuildmat

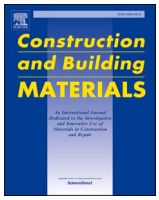

Energy-absorbing particles for enhanced mechanical performance of asphalt's aggregate skeleton

Laura Traseira-Piñeiro [a], Mahdi Bodaghi [b,*], Athina Grizi [c], Alvaro Garcia-Hernandez [d], Gabriele Albertini [a,*]

[a] Nottingham Transportation Engineering Centre, Department of Civil Engineering, University of Nottingham, Nottingham NG7 2RD, UK
[b] Department of Engineering, School of Science and Technology, Nottingham Trent University, Nottingham NG11 8NS, UK
[c] Region of Western Greece, Patras 26443, Greece
[d] Lehrstuhl und Institut für Straßenwesen, Aachen University, Aachen 52074, Germany

ARTICLE INFO

Keywords:
Cellular capsules
Asphalt self-healing
Energy absorption
Mechanical metamaterials

ABSTRACT

This paper evaluates the feasibility of using 3D-printed lattice metamaterials as an alternative to capsules containing rejuvenators to enhance the self-healing capability of asphalt. The original purpose of these capsules is to encapsulate a rejuvenator and ensure its gradual release under load. However, the cellular structure of the capsules, along with their inherent energy absorption properties, may have a non-negligible physical impact on the asphalt's aggregate skeleton, which is not well understood but could influence the asphalt performance. To address this, lattice structures with a wide range of stiffness, strength, and energy-absorption properties were firstly designed and 3D-printed. Subsequently, the mechanical behaviour of a composite granular medium composed of granite aggregates and either cellular capsules or 3D-printed lattices was investigated. Cyclic and monotonic experiments were conducted on this composite granular medium, which represents the aggregate skeleton of asphalt. Lastly, its mechanical response, plastic deformation of lattices and capsules, and the crushing behaviour of aggregates were measured. Through a comparative analysis of results obtained from lattices with significantly different mechanical and energy-absorption properties, it was found that: i) capsules do induce physical changes to the aggregate skeleton of asphalt; ii) despite design constraints, lattice metamaterials can be successfully 3D-printed and tailored to meet specific requirements; iii) Voronoi lattices emerge as a potential alternative to replace the capsules.

1. Introduction

In the UK, asphalt mixtures are used on 95% of road pavements, with an approximate annual production of 25 million tonnes [1]. This material is composed of graded aggregates, which provide stiffness and resistance to cumulative deformations, and a bituminous binder. Because of their viscoelastic properties, bitumen-bound materials can flow within the bitumen-filler mortar, reducing the risk of cracking due to temperature fluctuations or foundation settlements. However, an inadequate selection of the bituminous binder type and grade may also lead to permanent deformations, known as asphalt rutting [2–4].

In addition to the mixture design, the properties of the aggregates, which are the largest constituent of asphalt mixtures, will substantially affect asphalt's performance [3–5]. The interactions within the particles, their frictional forces and resistance to cracking are influenced by their geometrical properties, the type of aggregate and origin. Angular particles and rough textures increase the internal friction; elongated aggregates are more susceptible to cracking. The aggregate size, which is correlated with the surface area, influences the amount of binder required to coat the particles. The variability associated with the aggregates will also increase the difficulties in predicting the pavement lifespan [1–5].

However, pavement engineering has advanced significantly over the past decades, with new design approaches and alternative materials to make more sustainable asphalt roads while enhancing their performance: Warm-mix and cold-mix asphalts use bitumen additives and emulsions to lower the manufacturing temperatures, and their rheological properties can be altered as well by polymer modification, antioxidants or adhesion agents, among others [3,6–9]. There is an increasing interest in alternatives to natural aggregates, such as recycled

* Corresponding authors.
E-mail addresses: mahdi.bodaghi@ntu.ac.uk (M. Bodaghi), gabriele.albertini@nottingham.ac.uk (G. Albertini).

https://doi.org/10.1016/j.conbuildmat.2024.135055
Received 5 October 2023; Received in revised form 27 December 2023; Accepted 13 January 2024
Available online 24 January 2024

aggregates, industrial waste products like steel slag or fly ash, or crumb rubber from used tyres [3,10–14]. Moreover, recycled plastics with high melting points are being evaluated to replace part of the aggregate skeleton of asphalt mixtures, renamed as "plastiphalt" [12,15–18]. Lastly, some recent studies assessed 3D-printing aggregates or creating artificial aggregates with Additive Manufacturing (AM) techniques for an accurate reproduction of the aggregate's geometry [19–21], but also explored the use of new shapes and the effect of novel external geometries on the aggregate packing and stress response [22,23].

There has been extensive research conducted on encapsulated rejuvenators to increase asphalt's lifespan [24]. This technological innovation is based on promoting asphalt's self-healing by means of a rejuvenator that is progressively released from the capsules' polymeric matrix in which it is stored [25,26]. Thus, bitumen ageing, which causes asphalt to become stiffer and prone to cracking, can be controlled, and the binder regains its ability to flow and close any microcracks. Several rejuvenators and encapsulation processes were evaluated and, to achieve satisfactory laboratory results, the capsules were experimentally optimised, focusing on the release of the rejuvenator and the subsequent crack-healing [27–30]. Recent research, however, assessed the influence of the encapsulating structure itself, and the latest results suggest that embedded capsules have a non-negligible mechanical effect on asphalt's performance.

These studies [31,32] showed that the addition of cellular capsules was able to mitigate asphalt ravelling on unaged specimens subjected to cycles of impact loading of short test duration (about 10 min) with the Cantabro test. As the testing time was insufficient for the rejuvenator to diffuse and promote asphalt self-healing, the mitigation of asphalt ravelling was attributed to the cellular capsules' ability to undergo gradual collapse and absorb energy. According to the authors, the absorption of impact-load energy led to the deformation of the capsules, thereby increasing the pore pressure and promoting bitumen drainage, inducing to a local re-compaction. Moreover, the authors further suggested that this new mechanism may explain previous evaluations of asphalt self-healing through polymeric capsules containing asphalt rejuvenators [31]. Additionally, one of the most recent publications examined the influence of several variables during asphalt manufacturing on the energy absorption of the capsules in Stone Mastic Asphalt (SMA) produced at an asphalt plant. It was found that the binder content influences the performance of the capsules and, to maximise their effectiveness, capsules shall constitute part of the aggregate skeleton that characterises this type of asphalt mixture rather than float in the mastic [32].

The distinct properties of porous structures were initially studied by Gibson & Ashby, who referred to them as "cellular solids" after using the term "cell" to describe their structure, composed of interconnected beams or surface elements that conform the edges and faces of the unit cells [33]. Among other outstanding properties, these lightweight structures can withstand significant deformations at an almost constant stress under compression loading, exhibiting an excellent energy-absorption performance; their porous structure made of multiple unit cells makes them suitable for acoustical and thermal insulation; and their vast surface area and pore connectivity can be used in multiple fluid and biomedical applications [33–35]. Although several classifications have been proposed over time, they can be broadly categorised into foams, which have a random cell formation and distribution, and honeycombs (or 2D lattices) and 3D lattices, which have periodic patterns of unit cells [36–38]. Honeycomb and foams, which can be commonly found in nature, (e.g. cork or trabecular bone) were among the first cellular materials to be studied, and then, in light of the recent advances in Additive Manufacturing (AM), the focus changed towards architecting lattice structures with more complex geometries [37,39].

Hence, nowadays lattice structures are commonly employed in the design of metamaterials to obtain enhanced mechanical properties that are mainly associated with their microstructure, including the type, size, and arrangement of their cells, rather than the material composition [41]. They can be architected to offer a lightweight design, dissipate heat, provide high deformation resistance, or enhance the energy absorption and damping properties, among others. Moreover, numerical modelling can be used to optimise the internal structure of the lattices to attain the required mechanical properties, becoming an effective alternative to conventional experimental optimisations [37–43]. Lattice metamaterials have potential application in civil engineering, such as improving the structural and material performance, protecting infrastructure from impact and seismic damage or reducing noise and vibration pollution, as summarised in Fig. 1 [44–55].

The aim of this paper is to investigate whether cellular capsules, originally designed to promote asphalt self-healing through the release of asphalt rejuvenators, induce physical changes in the aggregate skeleton due to their energy absorption properties, ultimately affecting asphalt's performance and durability. This paper also evaluates the use of lattice structures that absorb energy as an alternative to the cellular capsules due to the advantages they offer in the design, optimisation, and manufacturing processes. To test this hypothesis, several 3D-printed particles with a lattice-based microstructure were designed, manufactured, and characterised. Then, a composite granular media comprising single-size aggregates was used to conduct a fundamental study. The monotonic and cyclic mechanical response of the composite granular media containing energy-absorbing particles, including the cellular capsules used in prior research, the selected lattice structures and Nylon spheres with high stiffness and negligible energy absorption was evaluated, as well as the deformation of the particles and the crushing behaviour of the aggregates.

2. Methodology

2.1. Experimental plan

The experimental plan was divided into the following phases:

The first phase consists in lattice characterisation, testing and selection. During the phase, diverse lattice structures were designed, 3D-printed, and mechanically characterised through uniaxial compression under a constant displacement rate. Two lattice structures with distinctly different mechanical properties were then selected for further evaluation in the second phase.

The second phase consists in a fundamental study of composite granular media containing energy-absorbing particles. In this phase, cellular capsules, spheric lattices and hard spheres were tested in a granular unbounded medium under static and cyclic compression loading. This fundamental study aimed to evaluate and compare the effect of the energy-absorbing particles on the overall response of composite granular unbounded media, as well as the deformation of the particles and the crushing behaviour of the granite aggregates.

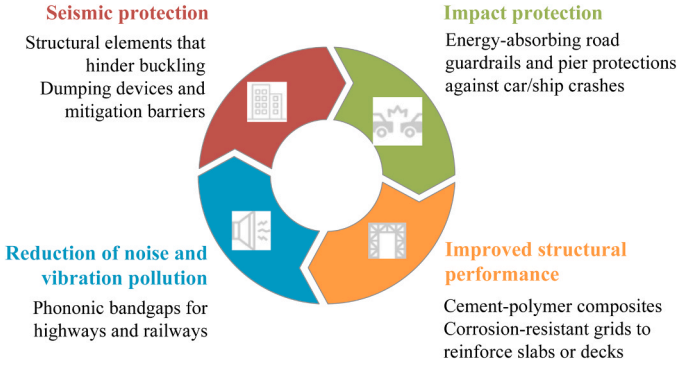

Fig. 1. Potential applications of lattice metamaterials in civil engineering.

2.2. Lattice materials, design, and fabrication

The lattices were 3D-printed by Multi Jet Fusion (MJF) using polyamides PA11 (particle size of 50 μm, powder melting point of 200 ^{o}C) and PA12 (particle size of 60 μm, powder melting point of 187 ^{o}C). PA12 is an oil-based polyamide obtained from petrochemical sources, whereas PA11 is a bio-based polyamide with a lower carbon footprint, usually synthesised from castor plants or other renewable sources. However, both thermoplastics possess a similar chemical structure, composed of amide groups (CO-NH) separated by 10 (PA11) or 11 (PA12) methylene groups (CH_2) [56]. They present a remarkable performance in terms of mechanical strength, fatigue, impact resistance, and abrasion resistance. Notably, PA11 stands out due to its enhanced elongation at break, superior chemical and ageing resistance and lower moisture absorption [57]. Both polyamides are heat-resistant and show an adhesion to bituminous binders like that of granite aggregates [19]. Furthermore, due to the wide range of temperatures between their melting and crystallisation points during manufacturing, PA11 and PA12 are excellent for printing parts with geometric complexity [56]. These polyamides were characterised by tensile testing using dumb-bell-shaped type 1B specimens from BS EN ISO 527–2:2012 [58].

As to the selected Additive Manufacturing (AM) technique, MJF provides fast printing with great accuracy and does not require any support. Moreover, the parts 3D-printed using MJF are practically isotropic and, therefore, their mechanical properties are not affected by the orientation of the part during the 3D-printing process [59].

As to the lattice design, it was restrained by the tolerance of the additive manufacturing technique, approximately 1 mm, and the maximum size of the aggregates used in the Stone Mastic Asphalt (SMA) mixtures that contain cellular capsules, which is 10 mm. Hence, the minimum thickness of the beams and surfaces was limited to approximately 1 mm and the enclosing volume of the lattice to a cube of 10x10x10 mm^3, as the preferred geometries for compressive testing are right prisms or specimens with a square or circular cross-section [60]. The generation process of periodic lattices is summarised in Fig. 2, and started with the selection of different beam-based or walled Triply Periodic Minimal Surface (TPMS) unit cells. Then, to generate lattices with the same microstructure and different relative densities, three sizes were considered for the unit cells. Lastly, these arrangements of cubic unit cells were centred in the previously defined enclosing volume, see Fig. 2. Stochastic lattices, on the other hand, were generated using Voronoi tessellations and required defining the number of points and randomness of the points in the enclosing volume to generate the inner

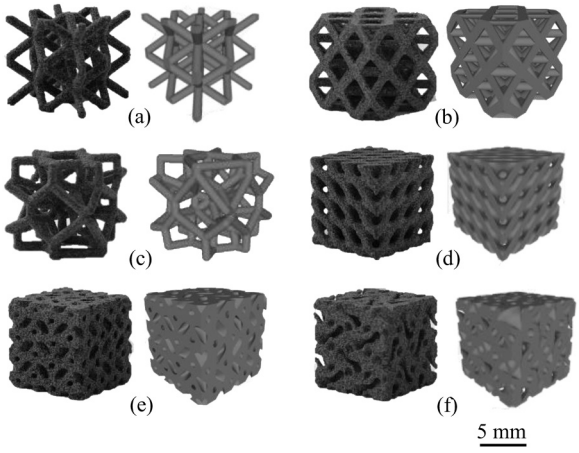

Fig. 3. Lattices before and after printing: (a) BCC, (b) Octet, (c) Voronoi, (d) Diamond, (e) Splitp and, (f) Lidinoid.

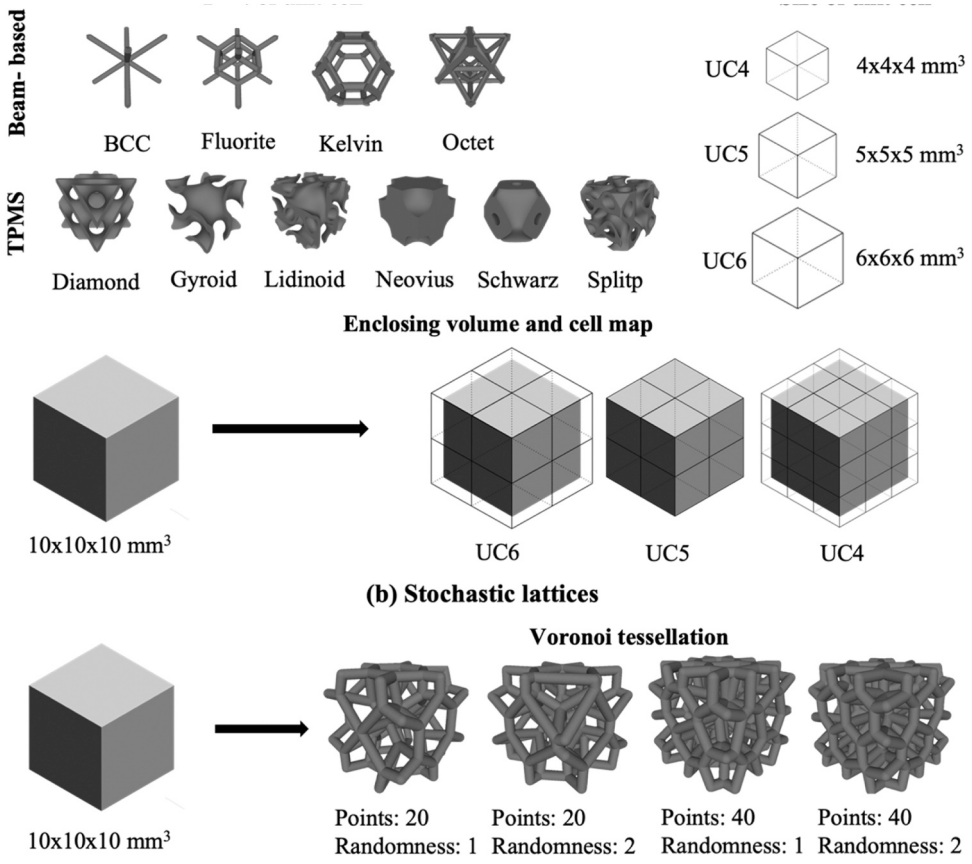

Fig. 2. Generation of: (a) Periodic metamaterials (beam-based lattices and walled TPMS) and (b) non-periodic metamaterials (Voronoi tessellation).

polygons, see Fig. 2 and Fig. 3.

Lastly, the thirty-four geometries generated were discretised to obtain closed, oriented, manifold, and not self-intersecting triangular meshes for the manufacturing process. The relative density of the lattices, ρ^*, was also calculated from the generated meshes, see Eq. (1). The two lattices selected for the fundamental study in a granular unbounded media were generated and 3D-printed following the same steps but using a spheric enclosing volume instead.

$$\rho^* = \frac{Volume\ \ of\ \ the\ \ lattice}{Enclosing\ \ \ volume} \tag{1}$$

2.3. Cellular capsules, materials, and fabrication

The cellular capsules used in this study were manufactured with the materials and upscaled encapsulation procedure proposed in [32]. The external ionic gelation technique was used to cross-link sodium alginate in the presence of calcium chloride, generating a cellular structure composed of calcium alginate, in which the oil-based rejuvenator can be stored. After the drying process, the average diameter of the cellular capsules was 1.7 mm ±0.3 standard deviations, and an average yield load of 9.5 N ±3 standard deviations.

2.4. Mechanical characterisation of the lattices

The base materials were characterised through tensile testing following BS EN ISO 527–1:2019 [61]. Five specimens of each type were tested on an Instron 5969 with a 50 kN load cell at 20 °C, at a loading rate of 0.5 mm/min (10% gauge length/min), and an optical extensometer was coupled to the equipment to evaluate the strain, expressed as the relative increase of the gauge length. Then, based on the measured stress-strain curve, the maximum stress and strain were calculated, as well as Young's modulus, E.

As to the designed lattice structures, multiple analyses can be conducted on the compressive stress-strain curves to reveal key properties of their energy absorption (W), and both loading and unloading characteristics have a major impact on the lattices' performance in most applications. The energy absorbed by a cellular structure up to a certain strain (ε_m) is represented by the area underneath the compressive stress-strain curve (σ-ε) [62], see Eq. (2), and the efficiency in the energy absorption ($\eta(\varepsilon)$) can also be calculated from the stress-strain curves, as the ratio of energy absorbed up to a certain strain divided by the stress itself, see Eq. (3) [63].

$$W = \int_0^{\varepsilon_m} \sigma(\varepsilon) d\varepsilon \tag{2}$$

$$\eta(\varepsilon) = \frac{1}{\sigma(\varepsilon)} \int_0^{\varepsilon_m} \sigma(\varepsilon) d\varepsilon \tag{3}$$

When subjected to uniaxial compression, an ideal energy absorber will present a rigid behaviour, showing no strain until a certain level of stress is reached, to then reveal an increasing strain at a constant stress, exhibiting a linear relationship between the strain and the energy absorption efficiency, see Fig. 4a, reaching 100% of efficiency at 100% of strain (ε_1). Lattice structures, however, often present three regimens, see Fig. 4b and c: i) A linear elastic region due to the initial bending of the cell edges, ii) a stress plateau in which the cell edges collapse by elastic bucking, plastic yielding, or brittle fracture at relatively constant stress and, iii) a densification region caused by the contact between the cell edges in which the stress has a steep rise while the energy absorption barely increases. Although the exact boundaries between those regions remain ambiguous, the efficiency in the energy absorption is frequently used to determine the onset densification strain (ε_{cd}) by identifying the

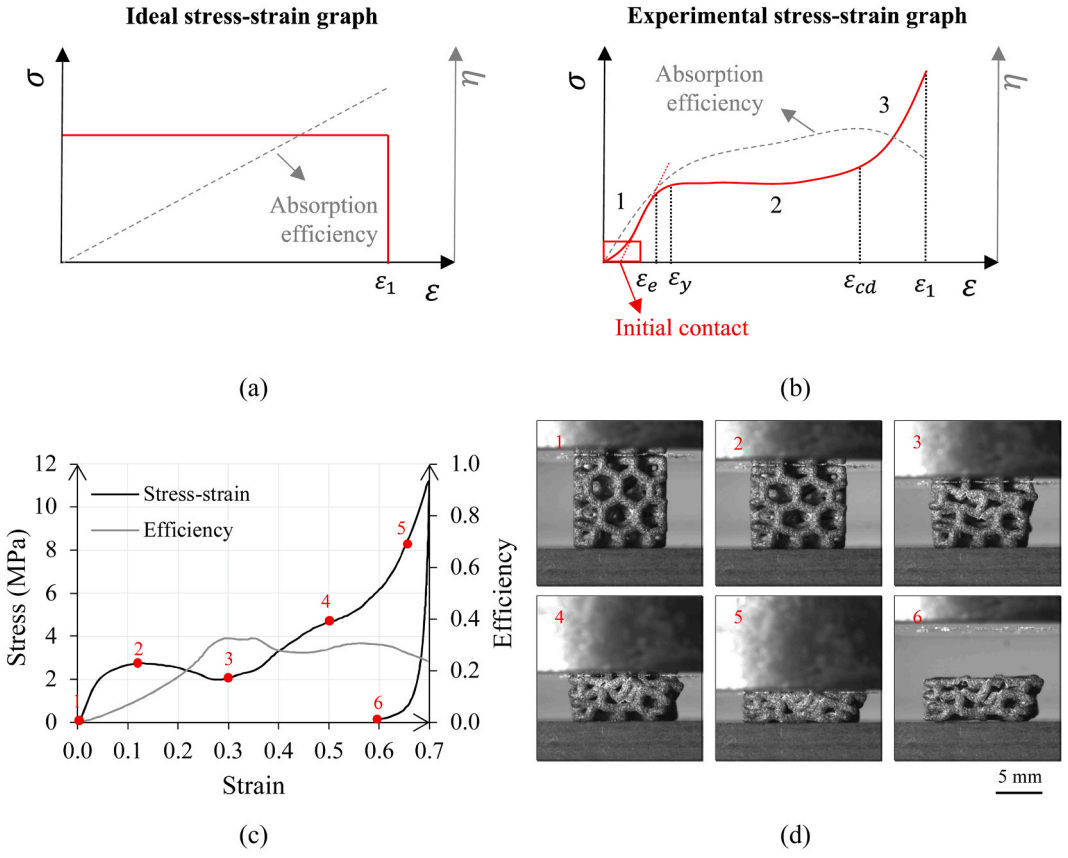

Fig. 4. Stress-strain and efficiency-strain graphs of (a) an ideal energy absorber, (b) an experimental energy absorber and, (c) a Voronoi lattice under uniaxial compression, with (d) photographs taken at different strain levels during testing.

maximum of the efficiency-strain graph, as shown in Eq. (4) [59].

$$\left.\frac{d\eta(\varepsilon)}{d\varepsilon}\right|_{\varepsilon=\varepsilon_{cd}} = 0 \tag{4}$$

Therefore, the designed lattices were characterised by uniaxial compression on three cubic specimens for each type, as recommended in [60]. The test was performed on the same equipment used for tensile testing, with a loading rate of 0.5 mm/min up to 70% of their initial height, followed by unloading at the same rate. The stress was then calculated by dividing the compressive load by the original cross-sectional area, while the strain was computed as the relative decrease in lattice height.

The Young's modulus was estimated from the elastic region of the stress-strain diagram, following the procedure defined in BS EN ISO 844 [60] to identify the steepest linear part within the range of 25% to 75% of the yield load prior to reaching 10% strain (ε_y). The indicated segment was divided into equal intervals and each segment's slope was calculated using the least square fit method to then identify the steepest linear region based on the highest sum of adjacent slopes [60]. The average strain in the plateau region (σ_{pl}) was calculated using Eq. (5), where ε_y (yield strain) was assumed to be 0.1 [59], and ε_{cd} (onset densification strain) was determined by the maximum efficiency method. The peak stress and total energy absorption at $\varepsilon_{0.7}$ (end of loading) were also calculated, as well as the recovered strain after the unloading phase. Lastly, the Pearson correlation coefficient was used to identify any correlation between the relative density of the lattices and the mechanical parameters obtained from their stress-strain graphs.

$$\sigma_{pl} = \frac{\int_{\varepsilon_y}^{\varepsilon_{cd}} \sigma(\varepsilon)d\varepsilon}{\varepsilon_{cd} - \varepsilon_y} \tag{5}$$

2.5. Evaluation of the lattice manufacturability and integrity

Before mechanical testing, the manufacturability of the designed lattices was evaluated to identify any printing irregularities that could compromise their performance, such as local printing inaccuracies in beam-based lattices or inaccurate geometries due to the wall thickness of the TPMS lattices. The equipment used was a digital inspection microscope (Inspectis HD-12) to obtain detailed views of the faces of the lattice structures, and then an optical microscope (Nikon Eclipse LV100ND) was used for a further evaluation of the printing irregularities. Regarding the structural integrity of the lattices, those that broke into several parts during compression testing, instead of experiencing a local collapse of the unit cells, were discarded from the selection to reduce the likelihood of particle breakage within the asphalt mixture and ensure a resilient granular media.

2.6. Mechanical response of a composite granular media containing energy-absorbing particles

Previous research suggested that, under loading, the cellular capsules deform in the contact areas with the aggregates, adapting their geometry to the surrounding aggregate skeleton while absorbing energy, inducing a local re-compaction [31]. But also, the binder content in the asphalt mixture may affect the capsule's ability to undergo deformation [32]. Therefore, a fundamental study was conducted to evaluate the lattice's deformation behaviour in a granular unbounded media, to reduce the variability associated with the presence of the binder on the lattice's deformation behaviour, as well as the potential challenges that may arise during the mixing process.

In addition, to further minimise gradation inconsistencies, single-size granite stones of 1–2 mm (bulk density: 1.22 g/cm^3) and 8–10 mm (bulk density: 1.32 g/cm^3) were used to evaluate the cellular capsules (bulk density: 0.63 g/cm^3) and the selected 3D-printed lattices (bulk densities of 0.24 g/cm^3 and 0.51 g/cm^3) respectively, ensuring that both granular media were geometrically similar [64]. Moreover, to discard the effect of introducing spheric particles on granite granular media, additional testing was performed using solid Nylon spheres made of PA66 (bulk density: 0.71 g/cm^3).

Uniaxial compression testing was performed on 75 mm height specimens enclosed in a cylindric steel container of 100 mm inner diameter [64] with plates on the top and base, see Fig. 5. Sample preparation included sieving, washing, and drying the aggregates, as well as calculating the average bulk densities of the aggregates and the energy-absorbing particles, following the guidelines from BS EN 1097–3:1998 [65]. Volumetric contents of 0% and 5% of energy-absorbing particles were used for the sample preparation [66], which included the use of a sieve shaker for 5 min to properly mix the particles with the aggregates, ensuring a uniform distribution on the granular medium. Then, samples were divided in half and compacted per layer, using a 2.5 kg compaction rammer [66,67] and applying four blows per layer using the pattern specified in [68], followed by 45 s in a vibration table for additional settling. Lastly, the top surface of the specimens was compacted again and levelled prior to placing the top plate.

Samples were stored and tested at room temperature (20 °C), and for the first phase of testing, uniaxial compression was applied at a constant displacement rate of 0.7 mm/min and up to a maximum load of 50 kN, see Fig. 5, subsequently followed by unloading at the same rate. Five specimens were tested per sample set, and then stress-strain curves were computed from the load and displacement readings to determine the average energy absorbed, see Eq. (2), and the average energy recovered.

During the second round of testing, the samples were subjected to cyclic loading after being preloaded with 0.1 kN, see Fig. 5. Samples containing 0% and 5% of cellular particles were tested over a range of loads (10, 20, 30, 40 and 50 kN) at 3 Hz for a total of 10,000 cycles, testing two specimens per sample set. Based on these test results, sample sets containing 0% and 5% of lattice spheres were tested under the maximum load, 50 kN, using four specimens per set. Lastly, after applying a moving average filter to ensure smoothness of the time-strain curves, the maximum test strain and the average deformation rate (in millimetres per hour) were calculated.

2.7. Analysis of materials after testing in a granular unbounded media

After cyclic testing, the aggregates were sieved to assess the influence of the energy-absorbing particles, including both the cellular capsules and the selected lattices, on the aggregate crushing behaviour. Additionally, the deformation of the energy-absorbing particles was evaluated by determining the equivalent diameter, aspect ratio and circularity before and after testing on sets of 30 samples.

2.8. Imaging techniques

Due to the size of the cellular capsules, an Environmental Scanning Electron Microscopy (Thermo Fisher FEI Quanta 650 ESEM), was used to obtain detailed views of the particles before and after testing in the granular medium. The sample preparation required fixing the particles to the sample holders with conductive carbon adhesive tape. Then, the equipment was operated with a vacuum level of 50 Pa, a beam voltage of 10 kV and a spot size of 5.

3. Results and discussion

3.1. Characterisation of materials used for MJF

Polyamides PA11 and PA12 gained significant popularity in powder bed fusion techniques such as MJF, and regardless of the similarities in their chemical structure, both materials exhibit different mechanical properties [69]. Therefore, to compare their material properties, the mechanical performance of both polyamides was assessed through

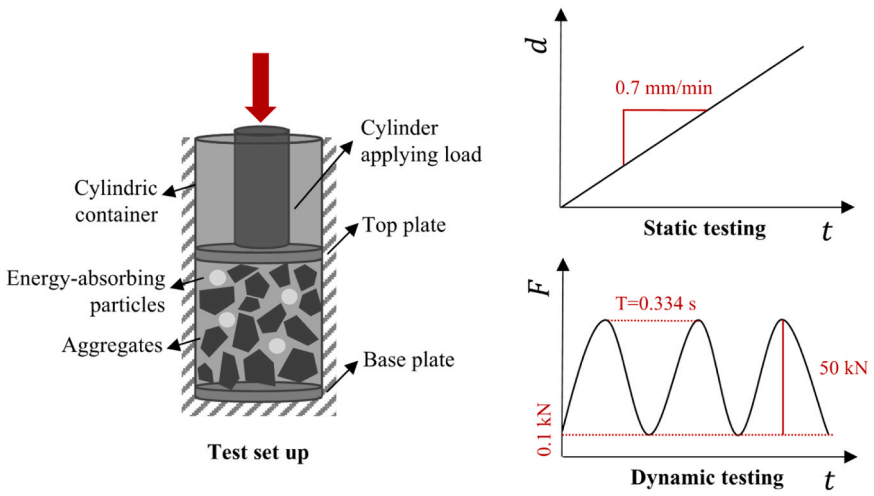

Fig. 5. Set-up for uniaxial compression testing of the unbounded granular media.

tensile testing, see Table 1. With a Young's modulus of $E = 1,209$ MPa, PA12 was more prone to elastic deformations than PA11 ($E = 1,402$ MPA). However, PA11 exhibited greater ductility, reaching higher tensile stress values at break and a maximum elongation of 67%, whereas PA12 only attained 15% elongation before breaking.

3.2. Manufacturability of the proposed lattices

Despite the design constraints, the excellent printability of the selected polyamides, coupled with the great accuracy provided by the MJF 3D-printing technology, enabled the successful manufacturing of the designed lattice structures. However, local printing inaccuracies were identified in several walled TPMS and beam-based lattices, regardless of the polyamide used, see Table 2. In the case of walled TPMS, surface points that did not attain the minimum thickness tolerance presented improper geometries, whereas some beam lattices yielded irregularities such as fused parts or imperfections at the end of the beams.

3.3. Evaluation of the lattice's mechanical performance

Due to the large number of lattices tested, the evaluation of their mechanical properties focused on the main attributes that characterise their stress-strain curves, which were plotted against their relative densities, following the methodology used in prior research studies [70], based on the Ashby plots [34]. Lattices that presented manufacturability difficulties were not included on this assessment, see Table 2, not only due to the inconsistent results they might lead to during their mechanical characterisation, but also because of the discrepancies between the original design and the 3D-printed lattices [72], which might compromise the use of numerical modelling for further evaluation and optimisation in future research. Moreover, lattices that fragmented into several pieces during mechanical testing were also discarded from further evaluation, see Table 2, to reduce the likelihood of particle breakage within the asphalt mixture, which must be composed of a durable granular media resistant to fragmentation.

Table 1
Results from tensile testing.

		PA11	PA12
E (Mpa)	Average	1401	1208
	St.dev.	80.8	16.4
Max stress (Mpa)	Average	50.1	42.5
	St.dev.	0.90	0.99
Max strain (-)	Average	0.67	0.15
	St.dev.	0.07	0.02

Table 2
Lattices discarded due to manufacturability (M) or integrity (I) issues.

Material	PA11			PA12		
Cell size	UC4	UC5	UC6	UC4	UC5	UC6
Diamond	I	I	M			M
Gyroid						
Lidinoid		M	I		M	
Neovius						
Schwarz	M		M	M		M
Splitp	M			M		
BCC	M, I		I	M, I		I
Fluorite	M		M, I	M		M
Kelvin			I		I	I
Octet		I				I
Material	**PA11**			**PA12**		
Voronoi P20.1						
Voronoi P20.2	I			I		
Voronoi P40.1	I					
Voronoi P40.2						

The test results are summarised in Fig. 6, and Table 3 provides a Pearson correlation matrix evaluating the selected parameters. In the linear elastic region of the stress-strain curves, the Young modulus exhibited a wide range of values, from 5 to 670 MPa (Fig. 6a), as well as the average stress in the plateau region, which ranged from 1.3 to 99 MPa (Fig. 6b), and the energy absorbed until the end of the plateau region, which variated from 0.6 to 60.9 J/cm^3 (Fig. 6c). Similarly, the peak stress at the maximum strain also covered a wide range of values, from 3.85 to 240 MPa (Fig. 6d). These four parameters were highly associated with the relative density of the lattices, as revealed by the Pearson correlation coefficients from Table 3.

Similar results were obtained in diverse research studies, in which it was acknowledged through the definition of scaling laws for each cell geometry [73] the relationship between the relative density of lattice structures and the mechanical properties extracted from the compressive stress-strain graphs, for both TPMS [74] and beam-based lattice structures [70]. However, the scaling laws do not isolate the effect of cell geometry from the relative density (also affected by the thickness of the beams/walls), which was also reported to affect the energy absorption properties of the lattices [59,75]. Regarding the selection of materials for MJF, although the overall lattice performance was similar when variating between PA11 and PA12, lattices manufactured with PA11 exhibited higher elastic modulus and stress values, which is aligned with the behaviour of the parent materials observed during tensile testing, that determine the baseline properties of the lattices [35], see Table 1.

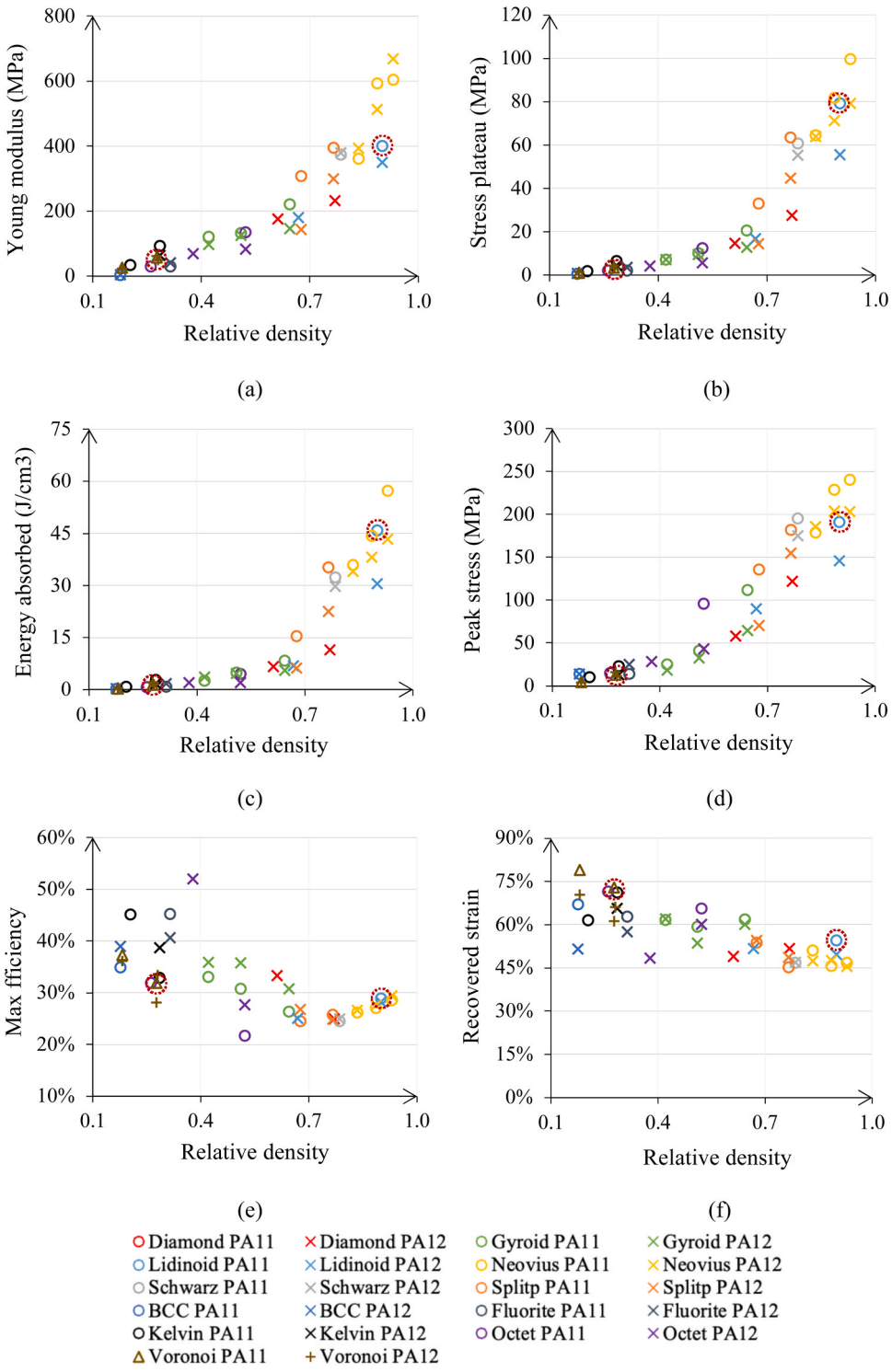

Fig. 6. Results from uniaxial compression of the lattices, and selected lattices for further evaluation (red dashed circles): (a) Young modulus, (b) average stress plateau, (c) energy absorbed, (d) peak stress, (e) maximum efficiency and (f) recovered strain.

Nonetheless, the magnitude of the correlation between the maximum efficiency and the recovered strain after 24 h of testing with the relative density of the evaluated lattice structures was found to be lower, see Table 3. Besides, Fig. 6e and f illustrate that, as the difference between the density of the lattice and its corresponding parent material grew, the dispersion in the test results increased as well. This indicates that the relative density is not the main parameter governing those mechanical properties, and thus, geometric properties inherent to each type of lattice cause an unneglectable effect on the lattice efficiency and recovered strain. Similar test results were obtained in [71], in which the efficiency in the energy absorption of several beam-based lattices printed with different AM processes yielded efficiency indexes in the same range of values (30–45%) without discerning a clear correlation with the relative density. Lastly, the influence of the type of polyamide was almost negligible for lattices with relative densities above 0.7, see Fig. 6e and f, whereas, below that range, lattices manufactured with PA11 exhibited greater recovered strain and lower efficiency in the energy absorption when compared to those manufactured with PA12.

Table 3
Pearson correlation coefficients.

	Relative density	Young modulus	Energy absorbed	Stress plateau	Peak stress	Max efficiency	Recovered strain
Relative density	1.00	0.91	0.86	0.89	0.93	-0.67	-0.79
Young modulus	0.91	1.00	0.96	0.97	0.96	-0.56	-0.74
Energy absorbed	0.86	0.96	1.00	1.00	0.95	-0.51	-0.71
Stress plateau	0.89	0.97	1.00	1.00	0.97	-0.54	-0.72
Peak stress	0.93	0.96	0.95	0.97	1.00	-0.65	-0.76
Max efficiency	-0.67	-0.56	-0.51	-0.54	-0.65	1.00	0.32
Recovered strain	-0.79	-0.74	-0.71	-0.72	-0.76	0.32	1.00

3.4. Lattice selection for testing in a granular media

The selected 3D-printing technologies allowed the successful manufacturing of lattice structures with a wide range of geometrical and mechanical properties from the same parent materials, see Fig. 6, although several lattices were discarded from further evaluation due to printing inaccuracies after manufacturing or integrity issues during uniaxial compression, see Table 2. Based on the results from Table 3, which identified a high correlation between the relative density of the lattices and four out of six parameters characterising their mechanical behaviour, the relative density was divided into two centred intervals, [0.20, 0.45] and [0.65, 0.90], aiming to select for further evaluation two lattice structures with distinct mechanical behaviours and thus, conduct a more comprehensive analysis. In the first interval, the maximum strain recovery was prioritised, whereas in the second interval, the focus shifted towards optimising the efficiency in the energy absorption. Based on this screening criteria, the Voronoi tessellation (ρ^*= 0.28, PA11), with recuperated about 73% of the strain after testing, and the Lidinoid (ρ^*= 0.9, PA11), with exhibited a maximum efficiency in the energy absorption of 29%, see Fig. 6, were selected for testing in a granular unbounded medium, aiming to evaluate the feasibility of using lattice structures as an alternative to cellular capsules.

Prior to this fundamental study, both lattices were subjected to cyclic uniaxial compression. Cubic samples were loaded under a constant displacement rate of up to 50% of strain, and for every 10% of strain, they were unloaded at the same displacement rate until reducing the vertical strain by 5%, generating with this loading-unloading profile the hysteresis loops depicted in Fig. 7. The deformation characteristics of the Voronoi tessellation were affected under repeated loading conditions, as depicted in Fig. 7a, resulting in a reduction of its bearing capacity. This might be attributed to the accumulated damage in the lattice structure as the bending stresses in the struts initiate and propagate cracks, which can be discerned in Fig. 4b, caused by the cell topology that significantly affects the fatigue properties of the Voronoi lattice, as reported by [72]. In contrast, the Lidinoid lattice displayed minimal differences in the stress-strain curve under cyclic loading, see Fig. 7b, exhibiting consistent behaviour on the hysteresis loops, which reveal a constant energy dissipation capacity.

3.5. Mechanical response in granular unbounded media

The test results from evaluating the mechanical response of granular unbounded media with and without energy-absorbing particles under a constant displacement rate are presented in Fig. 8. Single-size aggregates of 1–2 mm attained an average strain at the end of loading of 9.8%, as depicted in Fig. 8a, which increased up to 11.9% when capsules were incorporated into the granular media, increasing the energy absorbed by 24%, see Fig. 8b. However, as shown in Fig. 8a, the unloading force-strain curves remained parallel regardless of the cellular particle content, with no discernible differences in the energy recovered, as seen in Fig. 8b.

Moreover, when evaluating the results of the 8–10 mm aggregates without any particles, both the average maximum strain after loading (approximately 9.2%) and the energy absorbed (0.28 J/cm^3), were similar to those seen on the 1–2 mm aggregates, as shown in Fig. 8c and d. Samples containing Voronoi and Lidinoid lattices yielded a similar response, increasing the total strain after loading to approximately 10.6%, see Fig. 8c, and the energy absorbed to 0.31 J/cm^3, although a significative overlapping in the standard deviations was observed in Fig. 8d. Lastly, the mechanical response of granular media was further evaluated by introducing spheres made of Nylon 66 (maximum stress of 80 MPa under tensile testing [76]) to assess the effect of introducing spheric non-deformable particles on the 8–10 mm granular media. However, no differences were observed in the energy absorption of tested specimens with and without these spheres.

Therefore, to provide a more comprehensive examination, additional testing was performed under cyclic loading. Firstly, different cyclic loads were used on specimens with an aggregate size of 1–2 mm, with and without cellular capsules, to determine the optimum test parameters. Then, based on the results from Fig. 9a, a load of 50 kN was selected for further evaluation, not only due to the lack of overlapping in the maximum strain after testing samples with cellular particle contents of 0% and 5%, but also due to the increased difference in the deformation rate, which was found to be 80% higher on test specimens containing capsules subjected to a cyclic load of 50 kN.

Thus, results from Fig. 9a seem to suggest that the addition of cellular particles affected the mechanical response of the granular media under

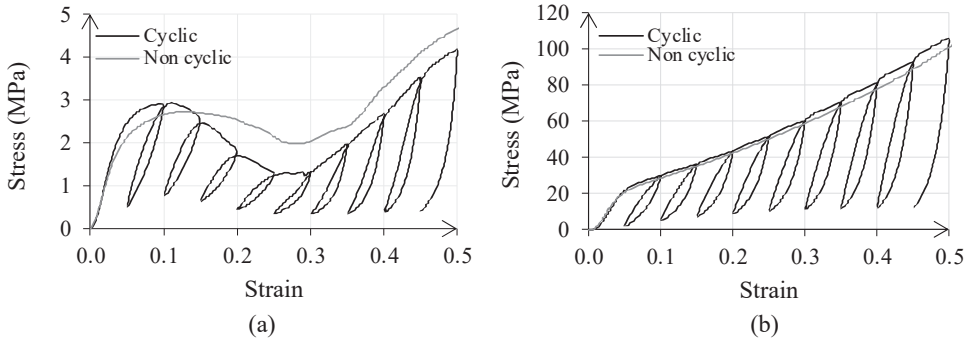

Fig. 7. Compressive stress-strain curve and deformation during mechanical testing of the selected lattices made of PA11: (a) Voronoi with 40 points and randomness 2 and, (b) Lidinoid with a unit cell size of 4 mm^3.

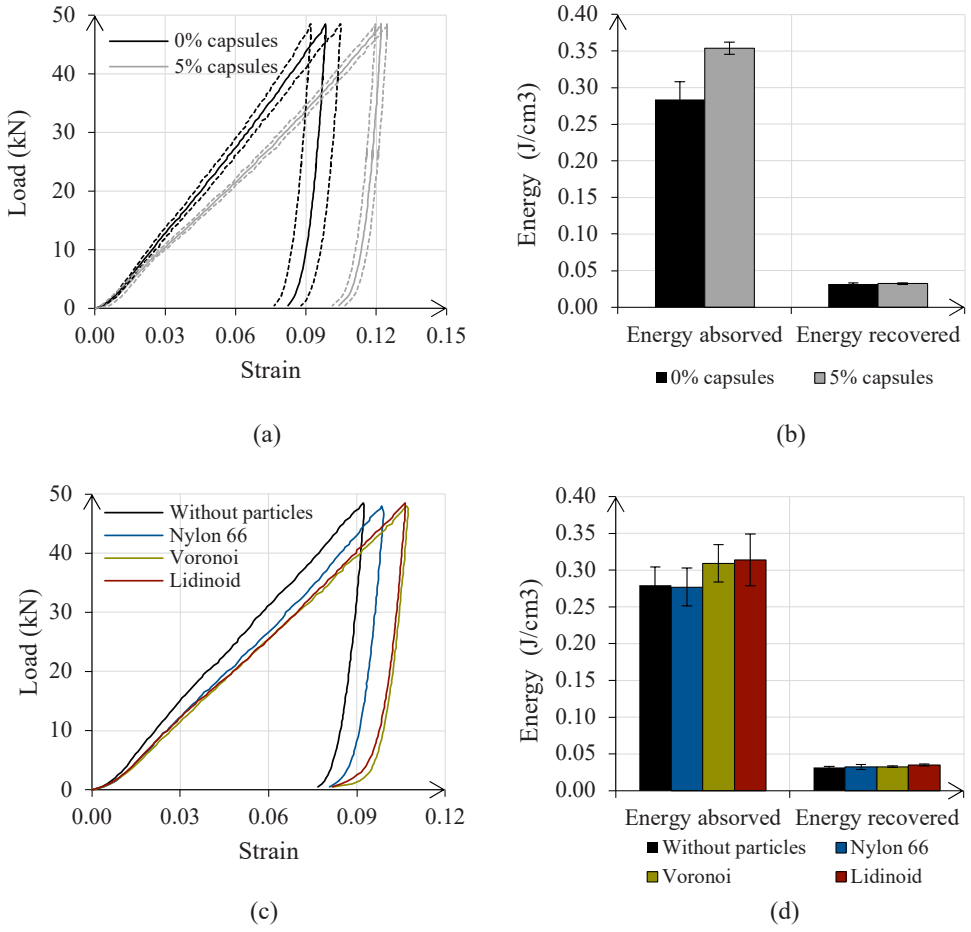

Fig. 8. Testing of the granular unbounded media under uniaxial compression: (a) Load -strain curves on samples containing cellular capsules, (b) energy absorption on samples containing cellular capsules, (c) load-strain curves on samples containing spheric lattices and (d) energy absorption on samples containing spheric lattices.

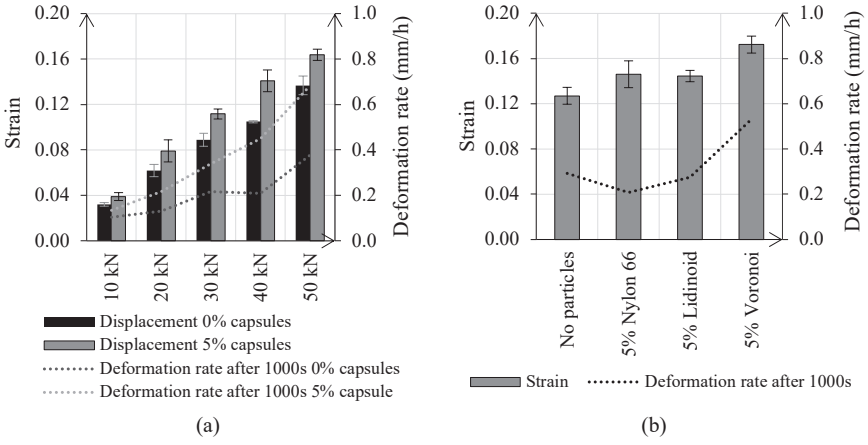

Fig. 9. Testing of the granular unbounded media under cyclic loading on: (a) samples containing cellular capsules and (b) samples containing spheric lattices.

cyclic loading, due to their progressive deformation during testing, which increased as well the strain and deformation rate of the granular unbounded media. As to the test results on specimens with an aggregate size of 8–10 mm, the addition of Voronoi lattices increased the total strain of the granular media, from 12% with 0% of particles to 17% on samples containing 5% of Voronoi lattices, see Fig. 9b. Besides, the displacement rate exhibited on samples containing Voronoi lattices increased by 80%, from 0.29 mm/h to 0.53 mm/h, showing a similar response to the addition of cellular capsules on the 1–2 mm granular media. However, Lidinoid lattices barely affected the deformation rate of the granular media, and the minimal impact they had on the total strain, see Fig. 9b, might be attributed to the presence of spheric particles in the granular media, as evidenced by the similar response showed by the spheres made of Nylon 66 in Fig. 9b.

To further support these findings, after cyclic testing the aggregates were sieved to evaluate the aggregate crushing, see Fig. 10, and the deformation of the energy-absorbing particles was assessed as well through imaging techniques, see Fig. 11 and Table 4. As to the Particle

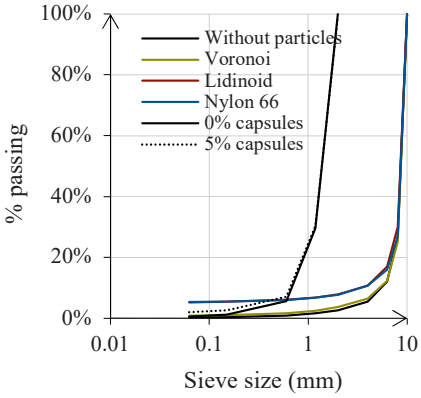

Fig. 10. Particle Size Distribution (PSD) curves after uniaxial compression under cyclic loading.

Size Distribution (PSD) curves, aggregates from samples that did not contain any energy-absorbing particles exhibited parallel curves that evidenced an equivalent behaviour. Besides, samples containing cellular capsules and Voronoi lattices did not show an increase in the percentage of crushed aggregates, see Fig. 10. However, the PSD curves of samples containing Lidinoid lattices and Nylon 66 spheres displayed a different response, showing a higher proportion of crushed aggregates that might be caused by the presence of spheres that did not absorb any energy and, therefore, contributed to that increase in the fraction of crushed aggregates.

The main outcomes obtained from analysing the response of the granular media under cyclic loading and evaluating the PSD curves of the aggregates were additionally supported by the assessment of the particle deformation in Table 4, through the measurement of the equivalent diameter, aspect ratio and circularity of the particles before and after testing. As shown in Fig. 11a and c, both cellular capsules and Voronoi lattices showed deformed particles after testing, and the shape descriptors used in Table 4 depicted sample sets statistically different before and after testing (P-value < 0.05). Lidinoid lattices and Nylon 66 spheres, however, did not evidence signs of a noteworthy deformation in Fig. 11b and d, or statistically significant changes on the shape descriptors evaluated in Table 4.

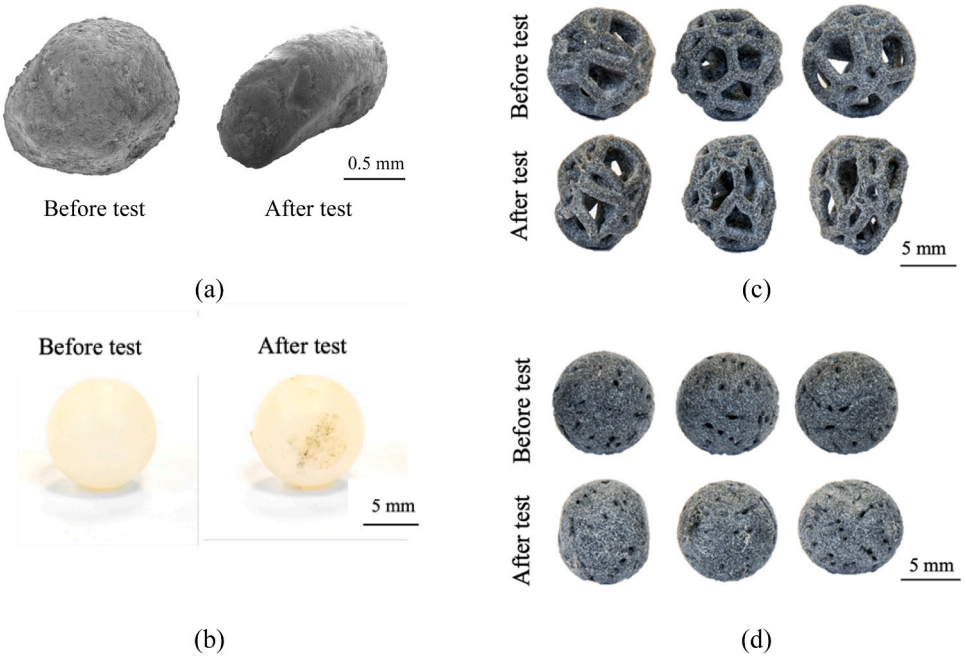

Fig. 11. Evaluated particles before and after testing(a) Images of the cellular capsules using the ESEM, (ii) photographs of spheres PA66 spheres, (c) photographs of Voronoi lattices and (c) photographs of Lidinoid lattices.

Table 4
Geometrical measurements of the evaluated particles before and after testing in a granular unbounded media.

	Diameter (mm)			Aspect Ratio (AR)			Circularity		
	Average	Stdev	P-value	Average	Stdev	P-value	Average	Stdev	P-value
Capsules									
Before	1.60	0.29	3.67E-06	1.31	0.22	7.59E-09	0.88	0.05	5.91E-16
After	1.77	0.27		1.54	0.35		0.81	0.08	
Voronoi									
Before	10.55	0.22	3.07E-30	1.05	0.03	6.49E-07	0.89	0.01	2.61E-02
After	8.99	0.63		1.12	0.06		0.88	0.04	
Lidinoid									
Before	10.50	0.18	4.47E-01	1.04	0.02	1.91E-01	0.90	0.00	3.69E-03
After	10.54	0.21		1.03	0.02		0.88	0.02	
Nylon 66									
Before	10.58	0.16	8.26E-01	1.04	0.03	8.52E-01	0.90	0.01	1.64E-02
After	10.59	0.26		1.04	0.02		0.90	0.00	

4. Conclusions

This paper investigated the use of lattice metamaterials as potential alternatives to the cellular capsules used in asphalt mixtures for asphalt-self healing and ravelling mitigation, with a specific focus on evaluating the physical impact of energy-absorbing particles on asphalt's aggregate skeleton with a fundamental study. Firstly, the materials used for 3D-printing the particles were characterised through tensile testing, and then, the mechanical response of lattice metamaterials was evaluated through uniaxial compression testing. Lastly, the effect of the cellular particles and the selected lattices on an unbounded granular media was assessed with a simplified study. This fundamental study encompassed the evaluation of the overall mechanical response of the granular media containing particles under static and cyclic loading, as well as the crushing behaviour of the aggregates and the deformation of the energy-absorbing particles. Based on the results of this research, the following conclusions were obtained:

- Despite the limitations imposed by the design constraints, the selected 3D-printing technologies and materials allowed the successful manufacturing of the lattice metamaterials.
- Lattice metamaterials offer a wide range of mechanical properties, which can be tailored to meet specific requirements. Although there was a high correlation between the relative density of the lattices and their mechanical response, the maximum efficiency and the recovered strain were also influenced by the lattice design itself.
- The fundamental study in a granular unbounded media verified the physical influence of the cellular capsules on the aggregate skeleton, corroborating findings from prior research.
- The Voronoi lattice emerged as a noteworthy alternative to the cellular capsules, showing an equivalent particle deformation and mechanical response of the granular media. Besides, 3D-printed lattice metamaterials offer advantages as to particle manufacturing using Multi Jet Fusion, and particle analysis and optimisation through numerical modelling.

5. Limitations and further study

This paper presented a fundamental study focused on evaluating the mechanical response of cellular capsules and lattice structures to uniaxial compression in an unbounded granular medium comprised solely of single-size stones, therefore excluding the impact of an aggregate gradation with different particle sizes and the effect of a bituminous binder on the performance of the energy-absorbing particles.

The results corroborated the findings from prior research [31], in which it was suggested that cellular capsules induce physical changes in the aggregate skeleton of the asphalt due to their energy absorption properties. In future research on cellular capsules, the focus shall be shifted from exploring the release and chemical influence of the encapsulated rejuvenator on asphalt self-healing to evaluating and optimizing the energy absorption of the capsule itself.

While this fundamental study identified noteworthy alternatives to the cellular capsules, it is essential to acknowledge its limitations, which should be addressed in future studies. These include the influence of forces and temperatures to which the lattice structures shall be exposed to during asphalt manufacturing on their physical and mechanical properties. It will also be crucial to investigate the response of lattice structures embedded in asphalt to loading under different load, temperature, and moisture conditions.

CRediT authorship contribution statement

Albertini Gabriele: Writing – review & editing, Writing – original draft, Supervision, Conceptualization. **Garcia-Hernandez Alvaro:** Writing – review & editing, Supervision, Funding acquisition, Conceptualization. **Bodaghi Mahdi**: Conceptualization, Methodology, Investigation, Writing – review & editing, Supervision. **Grizi Athina:** Writing – review & editing, Supervision. **Traseira-Piñeiro Laura:** Writing – original draft, Visualization, Investigation, Formal analysis, Data curation.

Declaration of Competing Interest

The authors declare that they have no known competing financial interests or personal relationships that could have appeared to influence the work reported in this paper.

Data availability

Data will be made available on request.

Acknowledgments

The authors acknowledge funding by Connect Plus M25 Ltd, express their gratitude to Bowman UK for their support during this research study, and thank the Nanoscale and Microscale Research Centre (nmRC) for providing access to the Environmental Scanning Electron Microscope.

References

[1] C. O'Flaherty, D. Hughes. Highways: the location, design, construction and maintenance of road pavements, 5th edition.,, ICE Publishing, London, 2016.
[2] Nick Thom. Principles of Pavement Engineering, 2nd edition.,, ICE Publishing, 2014.
[3] M.C. Forde, Institution of Civil Engineers (Great Britain), Ice manual of construction materials, Thomas Telford Limited, 2009.
[4] Robert N. Hunter, Asphalts in Road Construction, ICE Publishing, 2000.
[5] Robert N.Self Hunter, John Andy Read. Shell Bitumen Handbook, 6th edition.,, ICE Publishing, 2015.
[6] Y. Liu, P. Su, M. Li, Z. You, M. Zhao, Review on evolution and evaluation of asphalt pavement structures and materials, J. Traffic Transp. Eng. 7 (5) (2020) 573–599.
[7] S. Jain, B. Singh, Cold mix asphalt: an overview, J. Clean. Prod. 280 (2021) 124378.
[8] M.C. Rubio, G. Martínez, L. Baena, F. Moreno, Warm mix asphalt: an overview, J. Clean. Prod. 24 (2012) 76–84.
[9] M.R. Kakar, Z. Refaa, J. Worlitschek, A. Stamatiou, M.N. Partl, M. Bueno, Effects of aging on asphalt binders modified with microencapsulated phase change material, Compos. Part B: Eng. 173 (2019) 107007.
[10] S. Raschia, S. Tattolo, Use of alternative aggregates for the production of hot-mix asphalt surface layers: a performance evaluation, Constr. Build. Mater. 345 (2022) 128369.
[11] M. Al Mahbubi, E. Ahyudanari, Analysis the use of artificial aggregates as a substitute of coarse agreggates for surface of flexible pavement, J. Tek. ITS 8 (2) (2019) D47–D51.
[12] H. Robinson, A. Hulme, D. Day, Alternative aggregates in asphalt and concrete, Transportation Professional (2004).
[13] F. Moreno, M.C. Rubio, M.J. Martinez-Echevarria, Analysis of digestion time and the crumb rubber percentage in dry-process crumb rubber modified hot bituminous mixes, Constr. Build. Mater. 25 (5) (2011) 2323–2334.
[14] S.A. Tahami, A.F. Mirhosseini, S. Dessouky, H. Mork, A. Kavussi, The use of high content of fine crumb rubber in asphalt mixes using dry process, Constr. Build. Mater. 222 (2019) 643–653.
[15] Y. Ma, H. Zhou, X. Jiang, P. Polaczyk, R. Xiao, M. Zhang, B. Huang, The utilisation of waste plastics in asphalt pavements: a review, Clean. Mater. 2 (2021) 100031.
[16] S. Wu, L. Montalvo, Repurposing waste plastics into cleaner asphalt pavement materials: a critical literature review, J. Clean. Prod. 280 (2021) 124355.
[17] A. Hassani, H. Ganjidoust, A.A. Maghanaki, Use of plastic waste (poly-ethylene terephthalate) in asphalt concrete mixture as aggregate replacement, Waste Manag. Res. 23 (4) (2005) 322–327.
[18] S.E. Zoorob, L.B. Suparma, Laboratory design and investigation of the properties of continuously graded Asphaltic concrete containing recycled plastics aggregate replacement (Plastiphalt), Cem. Concr. Compos. 22 (4) (2000) 233–242.
[19] J. Liu, Z. Wang, X. Zhao, C. Yu, X. Zhou, Quantitative evaluations on influences of aggregate surface texture on interfacial adhesion using 3D printing aggregate, Constr. Build. Mater. 328 (2022) 127022.
[20] X. Wang, H. Wang, P. Feng, C. Wang, C. Zhang, A. Golroo, The movement property characterisation of coarse aggregate during gyratory compaction based on 3D-printed aggregate, Constr. Build. Mater. 361 (2022) 129608.
[21] W. Li, D. Wang, B. Chen, K. Hua, Z. Huang, C. Xiong, H. Yu, Preparation of artificial pavement coarse aggregate using 3d printing technology, Materials 15 (4) (2022) 1575.

[22] N.A. Conzelmann, M.N. Partl, F.J. Clemens, C.R. Müller, L.D. Poulikakos, Effect of artificial aggregate shapes on the porosity, tortuosity and permeability of their packings, Powder Technol. 397 (2022) 117019.
[23] A.G. Athanassiadis, M.Z. Miskin, P. Kaplan, N. Rodenberg, S.H. Lee, J. Merritt, H. M. Jaeger, Particle shape effects on the stress response of granular packings, Softw. Matter 10 (1) (2014) 48–59.
[24] Z. Deng, W. Li, W. Dong, Z. Sun, J. Kodikara, D. Sheng, Multifunctional asphalt concrete pavement toward smart transport infrastructure: design, performance and perspective, Compos. Part B: Eng. (2023) 110937.
[25] R. Micaelo, T. Al-Mansoori, A. Garcia, Study of the mechanical properties and self-healing ability of asphalt mixture containing calcium-alginate capsules, Constr. Build. Mater. 123 (2016) 734–744.
[26] T. Al-Mansoori, J. Norambuena-Contreras, R. Micaelo, A. Garcia, Self-healing of asphalt mastic by the action of polymeric capsules containing rejuvenators, Constr. Build. Mater. 161 (2018) 330–339.
[27] J. Norambuena-Contreras, E. Yalcin, A. Garcia, T. Al-Mansoori, M. Yilmaz, R. Hudson-Griffiths, Effect of mixing and ageing on the mechanical and self-healing properties of asphalt mixtures containing polymeric capsules, Constr. Build. Mater. 175 (2018) 254–266.
[28] S. Xu, A. Tabaković, X. Liu, E. Schlangen, Calcium alginate capsules encapsulating rejuvenator as healing system for asphalt mastic, Constr. Build. Mater. 169 (2018) 379–387.
[29] N. Ruiz-Riancho, A. Garcia, D. Grossegger, T. Saadoon, R. Hudson-Griffiths, Properties of Ca-alginate capsules to maximise asphalt self-healing properties, Constr. Build. Mater. 284 (2021) 122728.
[30] N. Ruiz-Riancho, T. Saadoon, A. Garcia, D. Grossegger, R. Hudson-Griffiths, Optimisation of self-healing properties for asphalts containing encapsulated oil to mitigate reflective cracking and maximise skid and rutting resistance, Constr. Build. Mater. 300 (2021) 123879.
[31] L.T. Piñeiro, T. Parry, F. Haughey, A. Garcia-Hernández, Architected cellular particles to mitigate asphalt stone loss, Constr. Build. Mater. 328 (2022) 127056.
[32] L. Traseira-Piñeiro, T. Parry, F. Haughey, A. Garcia-Hernandez, Performance of plant-produced asphalt containing cellular capsules, Materials 15 (23) (2022) 8404.
[33] L.J. Gibson, Cellular solids, Mrs Bull. 28 (4) (2003) 270–274.
[34] D. Bhate, C.A. Penick, L.A. Ferry, C. Lee, Classification and selection of cellular materials in mechanical design: engineering and biomimetic approaches, Designs 3 (1) (2019) 19.
[35] W. Tao, M.C. Leu, Design of lattice structure for additive manufacturing. In 2016 International Symposium on Flexible Automation (ISFA), IEEE,, 2016, pp. 325–332.
[36] C. Pan, Y. Han, J. Lu, Design and optimisation of lattice structures: a review, Appl. Sci. 10 (18) (2020) 6374.
[37] A. Nazir, K.M. Abate, A. Kumar, J.Y. Jeng, A state-of-the-art review on types, design, optimisation, and additive manufacturing of cellular structures, Int. J. Adv. Manuf. Technol. (2019).
[38] M. Bodaghi, N. Namvar, A. Yousefi, H. Teymouri, F. Demoly, A. Zolfagharian, Metamaterial boat fenders with supreme shape recovery and energy absorption/dissipation via FFF 4D printing, Smart Mater. Struct. 32 (9) (2023) 3489–3510, 095028.104(9).
[39] T.A. Schaedler, W.B. Carter, Architected cellular materials, Annu. Rev. Mater. Res. 46 (2016) 187–210.
[40] A. Nazir, K.M. Abate, A. Kumar, J.Y. Jeng, A state-of-the-art review on types, design, optimization, and additive manufacturing of cellular structures, Int. J. Adv. Manuf. Technol. 104 (2019) 3489–3510.
[41] X. Zhou, L. Ren, Z. Song, G. Li, J. Zhang, B. Li, Q. Liu, Advances in 3D/4D printing of mechanical metamaterials: from manufacturing to applications, Compos. Part B: Eng. (2023) 110585.
[42] C. Pan, Y. Han, J. Lu, Design and optimisation of lattice structures: a review, Appl. Sci. 10 (18) (2020) 6374.
[43] P. Jiao, A.H. Alavi, Artificial intelligence-enabled smart mechanical metamaterials: advent and future trends, Int. Mater. Rev. 66 (6) (2021) 365–393.
[44] X.Y. Zhang, X. Ren, Y. Zhang, Y.M. Xie, A novel auxetic metamaterial with enhanced mechanical properties and tunable auxeticity, Thin-Walled Struct. 174 (2022) 109162.
[45] Y. Zhang, X. Ren, X.Y. Zhang, T.T. Huang, L. Sun, Y.M. Xie, A novel buckling-restrained brace with auxetic perforated core: experimental and numerical studies, Eng. Struct. 249 (2021) 113223.
[46] J.A. Rosewitz, H.A. Choshali, N. Rahbar, Bioinspired design of architected cement-polymer composites, Cem. Concr. Compos. 96 (2019) 252–265.
[47] N. Friedman, A. Ibrahimbegovic, Overview of highly flexible, deployable lattice structures used in architecture and civil engineering undergoing large displacements, YBL J. Built Environ. 1 (1) (2013) 85–103.
[48] M. Saafi, design and fabrication of FRP grids for aerospace and civil engineering applications, J. Aerosp. Eng. 13 (4) (2000) 144–149.
[49] F. Sun, L. Xiao, Bandgap characteristics and seismic applications of inerter-in-lattice metamaterials, J. Eng. Mech. 145 (9) (2019) 04019067.
[50] Aguzzi, G., Colombi, A., & Chatzi, E.N. (2021). Vibration mitigation via octet lattice structures. In 3rd International Conference on Natural Hazards & Infrastructure (ICONHIC)(p. 228).
[51] Y. Nian, S. Wan, X. Wang, P. Zhou, M. Avcar, M. Li, Study on crashworthiness of nature-inspired functionally graded lattice metamaterials for bridge pier protection against ship collision, Eng. Struct. 277 (2023) 115404.
[52] Y. Darwish, M. ElGawady, Analysis of metamaterial bi-stable elements as energy dissipation systems, Bridge Struct. 15 (4) (2019) 151–159.
[53] X. Lu, X. Wu, H. Xiang, J. Shen, Y. Li, Y. Li, X. Wang, Triple tunability of phononic bandgaps for three-dimensional printed hollow sphere lattice metamaterials, Int. J. Mech. Sci. 221 (2022) 107166.
[54] Z. Gan, Y. Zhuge, D.P. Thambiratnam, T.H. Chan, T. Zahra, M. Asad, Recent advances in auxetics: applications in cementitious composites, Int. J. Prot. Struct. 13 (2) (2022) 295–316.
[55] S. Kaewunruen, V. Martin, Life cycle assessment of railway ground-borne noise and vibration mitigation methods using geosynthetics, metamaterials and ground improvement, Sustainability 10 (10) (2018) 3753.
[56] M. Bahrami, J. Abenojar, M.A. Martínez, Comparative characterisation of hot-pressed polyamide 11 and 12: mechanical, thermal and durability properties, Polymers 13 (20) (2021) 3553.
[57] L. Telen, P. Van Puyvelde, B. Goderis, Random copolymers from polyamide 11 and polyamide 12 by reactive extrusion: synthesis, eutectic phase behavior, and polymorphism, Macromolecules 49 (3) (2016) 876–890.
[58] British Standards Institution Plastics. Determination of tensile properties. Test conditions for moulding and extrusion plastics. BS EN ISO 527-2 2012 BSI, London.
[59] F.N. Habib, P. Iovenitti, S.H. Masood, M. Nikzad, Fabrication of polymeric lattice structures for optimum energy absorption using Multi Jet Fusion technology, Mater. Des. 155 (2018) 86–98.
[60] British Standards Institution Rigid cellular plastics. Determination of compression properties. BS EN ISO 844 2021 BSI, London.
[61] British Standards Institution Plastics. Determination of tensile properties. General principles. BS EN ISO 527-1 2019 BSI, London.
[62] M. Avalle, G. Belingardi, R. Montanini, Characterization of polymeric structural foams under compressive impact loading by means of energy-absorption diagram, Int. J. Impact Eng. 25 (5) (2001) 455–472.
[63] P. Drane, M. De Jesus-Vega, M. Inalpolat, J. Sherwood, N. Orbey, Inductive quantification of energy absorption of high-density polyethylene foam for repeated blunt impact, Proc. Inst. Mech. Eng. Part L: J. Mater.: Des. Appl. 234 (3) (2020) 531–545.
[64] Y. Xiao, M. Meng, A. Daouadji, Q. Chen, Z. Wu, X. Jiang, Effects of particle size on crushing and deformation behaviors of rockfill materials, Geosci. Front. 11 (2) (2020) 375–388.
[65] British Standards Institution, Tests for mechanical and physical properties of aggregates Determination of loose bulk density and voids. BS EN 1097-3:1998, BSI, London, 1998.
[66] Y. Guo, V. Markine, W. Qiang, H. Zhang, G. Jing, Effects of crumb rubber size and percentage on degradation reduction of railway ballast, Constr. Build. Mater. 212 (2019) 210–224.
[67] British Standards Institution, Methods of test for soils for civil engineering purposes. Classification tests and determination of geotechnical properties. BS 1377-2:2022, BSI,, London, 2022.
[68] ASTM Committee D-18 on Soil and Rock Standard Test Methods for Laboratory Compaction Characteristics of Soil Using Modified Effort (56,000 Ft-Lbf/Ft3 (2,700 KN-M/M3)) 1 2009 ASTM international,.
[69] M. Bahrami, J. Abenojar, M.A. Martínez, Comparative characterisation of hot-pressed polyamide 11 and 12: mechanical, thermal and durability properties, Polymers 13 (20) (2021) 3553.
[70] O. Al-Ketan, R.K.A. Al-Rub, R. Rowshan, The effect of architecture on the mechanical properties of cellular structures based on the IWP minimal surface, J. Mater. Res. 33 (3) (2018) 343–359.
[71] M. Mohsenizadeh, F. Gasbarri, M. Munther, A. Beheshti, K. Davami, Additively-manufactured lightweight Metamaterials for energy absorption, Mater. Des. 139 (2018) 521–530.
[72] T. Maconachie, M. Leary, B. Lozanovski, X. Zhang, M. Qian, O. Faruque, M. Brandt, SLM lattice structures: properties, performance, applications and challenges, Mater. Des. 183 (2019) 108137.
[73] S. Yuan, C.K. Chua, K. Zhou, 3D-printed mechanical metamaterials with high energy absorption, Adv. Mater. Technol. 4 (3) (2019) 1800419.
[74] M.M. Sychov, L.A. Lebedev, S.V. Dyachenko, L.A. Nefedova, Mechanical properties of energy-absorbing structures with triply periodic minimal surface topology, Acta Astronaut. 150 (2018) 81–84.
[75] I. Maskery, L. Sturm, A.O. Aremu, A. Panesar, C.B. Williams, C.J. Tuck, R.J. Hague, Insights into the mechanical properties of several triply periodic minimal surface lattice structures made by polymer additive manufacturing, Polymer 152 (2018) 62–71.
[76] S. Meister, D. Drummer, Influence of manufacturing conditions on measurement of mechanical material properties on thermoplastic micro tensile bars, Polym. Test. 32 (2) (2013) 432–437.